SAPIENZA

UNIVERSITA' DI ROMA

DOTTORATO DI RICERCA IN MEDICINA SPERIMENTALE
XXXIV CICLO

"Investigation of the molecular mechanisms underlying left ventricular hypertrophy in the presence of
Complex I deficiency-dependent mitochondrial dysfunction"

DOTTORANDO

Dr.ssa Giovanna Gallo
Matricola 1228239

DOCENTE GUIDA

Prof.ssa Speranza Rubattu

COORDINATORE DEL DOTTORATO
Prof. Maurizio Sorice

ANNO ACCADEMICO 2020/2021

Index

1. Background

1.a Pathophysiology of left ventricular hypertrophy

Left ventricular hypertrophy (LVH) is an initially adaptive process which occurs when the heart puts in place pathophysiological mechanisms to compensate an increased hemodynamic burden (1,2).

Indeed, in the presence of pressure and/or volume overload, the following compensatory processes may be involved:

(1) the Frank- Starling mechanism to increase crossbridge formation.

(2) augmentation of muscle mass to bear the extra load.

(3) recruitment of neurohormonal systems to increase contractility.

LVH is a consequence of the increase in size of existing cardiomyocytes rather than of hyperplasia due to cell proliferation, since cardiomyocytes become terminally differentiated soon after birth.

In response to pressure overload in conditions such as aortic stenosis or hypertension, the parallel addition of sarcomeres causes an increase in myocyte width, which in turn increases wall thickness (1,2). This remodeling produces concentric hypertrophy which consists in an increase in ratio of wall thickness/chamber dimension. This phenomenon occurs according to LaPlace's law which shows that the load on any region of the myocardium is given as follows: transmural pressure*radius/wall thickness (1,2). Consequently, an increase in pressure can be offset by an increase in wall thickness (Figure 1).

Figure 1. Pathophysiological mechanisms of LVH development

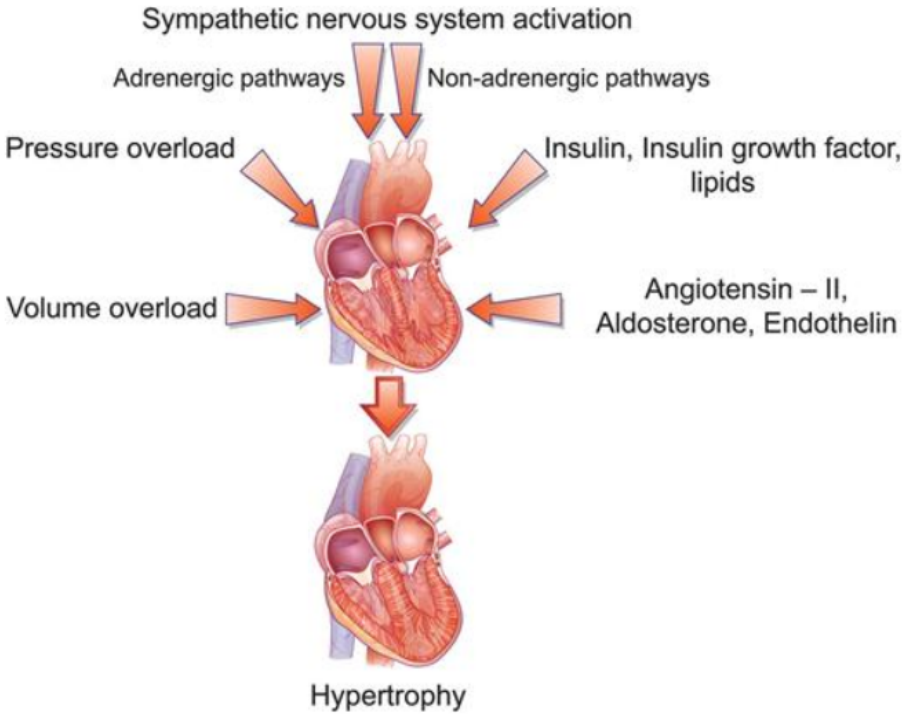

It has been shown that within hours after the occurrence of a pressure overload, myosin heavy chain synthesis increases by about 35% throughout a translational efficiency-2-mediated mechanism (3-7). If the increased afterload persists, complex changes in gene reprogramming occur, which include the re-expression of immature fetal cardiac genes that modify motor unit composition, regulation of energy metabolism, and that encode components of hormonal pathways such as atrial natriuretic peptide (ANP) and angiotensin converting enzyme (ACE). Moreover, a blunted expression occurs in other genes that modify intracellular ion homeostasis, namely the downregulation of sarcoplasmic reticulum calcium ATPase (SERCA-2), of β1-adrenergic receptors and M2 muscarinic receptors (3-7).

The downregulation of SERCA-2 is nearly ubiquitous in animal models of advanced pressure overload hypertrophy, and changes in SERCA-2 levels have been shown to modify the time course of the calcium transient, myocardial relaxation, and the force frequency response. In addition to

these changes, other molecular adaptations have been described to modify crossbridge attachment and perturb myocardial relaxation, including changes in troponin subunit isoform expression and phosphorylation, and blunted cAMP-mediated phosphorylation of regulatory proteins such as phospholamban (8,9).

Other switches include an increased expression of the slow myosin ATPase isoform β-myosin heavy chain relative to the fast myosin ATPase isoform α-myosin heavy chain with the initial aim to promote a more favorable energetic economy for myocardial cells (10).

Several mechanisms have been proposed to explain how the mechanical input produced by an increase in pressure load is transduced into a modified gene transcription in the nucleus. In this context, the focal adhesion complex, composed by integrins that connect the internal cytoskeleton of the cell, which is connected to the nucleus, to the extracellular matrix (ECM), may be involved (11-13). Indeed, multiple tyrosine-phosphorylated kinases and serine-threonine kinases that are implicated in the signaling of hypertrophy can be found in the ECM (14). In chronic conditions, changes of integrin expression and possibly integrin shedding into adjacent ECM have been shown, resulting in disordered biomechanical signal transduction for growth and suboptimal myocyte-ECM coupling for force generation (15). These modifications generate the recruitment of the G-protein–coupled neurohormones such as angiotensin II (ATII) and endothelin-1 (ET-1), whose activation amplifies the growth signaling triggered by the mechanical event itself (16,17). Indeed, ATII via its type 1 receptor (AT1R) plays an important role in the induction of hypertrophy directly inducing the molecular events of early cardiac growth (16,17). However, it has been shown that pressure overload is able to

produce cardiac hypertrophy also in transgenic mice with AT1R knockout, suggesting that ATII is not mandatory in this process (18).

Other studies have examined the role of calcineurin in the development of cardiac hypertrophy. Transgenic mice that overexpress components of the calcineurin signaling pathway develop a hypertrophic phenotype (19). However, calcineurin inhibitors have failed to suppress experimental hypertrophy in several animal models and in humans with hypertension after cardiac transplantation (20).

These observations suggest that different signaling pathways are probably involved in the modulation of load-induced hypertrophy, with the potential recruitment of alternate signaling cascades when a single pathway is suppressed (21).

Beside the growth of cardiomyocytes, the development of cardiac hypertrophy also involves the surrounding architecture of connective tissue, primarily composed of collagen with smaller amounts of elastin, laminin and fibronectin, and the capillary and nerve networks (22,23).

In the initial phases of pressure-overload hypertrophy, the increase in collagen production occurs as an adaptation to overload. However, if this condition persists, pathological collagen deposition, which is characterized by both perivascular and interstitial fibrosis, may occur. Some models have shown that reactive fibrosis may be triggered by defective cell-ECM contact or by the local activation of trophic peptides such as ATII, aldosterone, and/or catecholamines which activate the sequential expression of transforming growth factor-β1 (TGF-β1), fibronectin, and relative increase of collagen I (9,24).

According to these findings, chronic hypertrophy may be deleterious over the long-term. Indeed, changes in radius, thickness, and pressure are not

normalized and are regulated by negative feedback loops, this resulting in the development of exuberant hypertrophy and increased wall stress. In patients with LVH due to sustained pressure overload (hypertension and aortic stenosis) a hemodynamic hallmark is the elevation of LV end-diastolic pressure relative to a normal or small LV diastolic cavity volume, with a decrease in diastolic chamber distensibility and an increase in myocardial stiffness (25,26). Moreover, persistent cardiac hypertrophy is associated with disturbed energy metabolism. In such a context, mitochondria play a fundamental role in the production of the energy necessary for an adequate contraction and relaxation of cardiomyocytes to meet the workload demand (27). In fact, mitochondria are the main source of energy in eukaryotic cells and are abundant in high-energy-demanded organs like the heart. The quality of these organelles is controlled by remodeling mechanisms including biogenesis and repair, dynamics, and mitophagy. Under pathological conditions, the activities of ATP synthase and mitochondrial oxidative phosphorylation complex are attenuated, resulting in reduced production of ATP (28).

1.b The role of mitochondrial dysfunction in the development of LVH

An increasing body of evidence has shown that mitochondrial dysfunction might be associated with the development of cardiac hypertrophy (29,30). Indeed, the heart is particularly susceptible to mitochondrial dysfunction due to its strict dependence on aerobic metabolism and disruptions in mitochondrial bioenergetics might underlie a variety of chronic myocardial pathologies. A common feature of mitochondrial dysfunction in the heart is disruption of mitochondrial complex I (CI), known as NADH: ubiquinone oxidoreductase, caused either by mutation in the genes responsible of a fully functional complex or by cumulative damage to the complex itself (31).

Mitochondrial CI is the primary entry point for electrons into the mitochondrial respiratory chain and plays an essential role in generating the mitochondrial membrane potential. Electrons are donated from NADH to CI and then to other components of the chain to reduce molecular oxygen to form H_2O. Flow of electrons through the oxidative phosphorylation (OXPHOS) chain is accompanied by pumping of protons across the mitochondrial inner membrane, thus creating a transmembrane electrochemical gradient (32). CI leaks electrons in the intermembrane space to generate superoxide anion. Moreover, CI contributes to about 40% of the proton motive force that drives ATP synthesis by ATP synthase, and is a major source of mitochondrial anion superoxide production (Figure 2). A dysfunctional CI results in an increased mitochondrial reactive oxygen species (ROS) accumulation and deleterious cellular effects which may contribute to the development of cardiac hypertrophy (33).

Figure 2. Mitochondrial oxidative phosphorylation chain

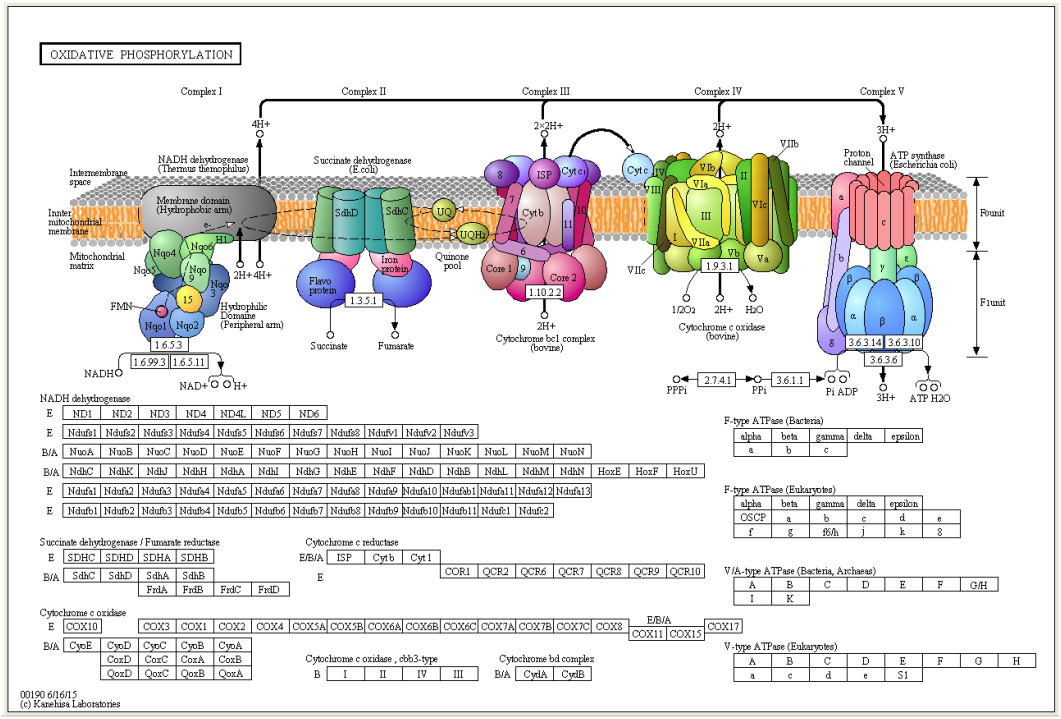

Mutations or deficiency of the NADH:ubiquinone oxidoreductase subunit S1 (Ndufs1), one of the core subunits of mitochondrial CI, destabilize CI assembly and result in defects of the activity of the electron transport chain (ETC) with decreased ATP production. The resulting mitochondrial damage activates the processes of fusion and fission to restore damaged mitochondria and to remove damaged mitochondrial fragments.

Ndufs1 also plays a central role in the regulation of morphological dynamics, of mitochondrial crista remodeling, cytochrome release, and mitochondrial respiration. Ndufs1 has been demonstrated to be significantly downregulated in heart tissue of mice with cardiac hypertrophy (34). Moreover, in vitro mechanistic studies showed that Ndusf1 knockdown induced cardiomyocyte hypertrophy, decreased mitochondrial DNA content and increased mitochondrial ROS production in cardiomyocytes (35). On the other hand, the overexpression of Ndusf1 in rat cardiomyocytes was able to counterbalance the pro-hypertrophic effects

of ATII detected by the over-expression of ANP, brain natriuretic peptide (BNP), and β-myosin heavy chain, which are commonly used as cardiac hypertrophic biomarkers (35). Other studies demonstrated that ATII treatment induced downregulation of Ndusf1 in the mouse heart and exacerbated mitochondrial dysfunction and oxidative stress to cause heart failure (HF) (36,37).

Also, the disruption of the Ndufs4 gene, which encodes a 18 kDa subunit of CI that plays a role in assembly or stability of the entire complex, has been associated to the development of cardiac hypertrophy. Indeed, the selective disruption of the Ndufs4 gene in the mouse heart led to a 50% decrease in CI activity, that in turn may drive to severe hypertrophic cardiomyopathy (38). In this model in which a partial CI disruption was performed through Ndufs4 ablation, MRI evaluation showed that LV ejection fraction (LVEF) was significantly lower in Ndufs4-null mice without sex-dependent differences, with a concomitant decrease in LV stroke volume and a significant increase in LV mass (38). No differences in hydrogen peroxide levels were detected between Ndufs4-null mouse hearts and controls. Moreover, the cleavage and activation of caspase 3, a marker of apoptosis, were comparable between knockout (KO) mice and controls (38). These findings might suggest that the development of hypertrophy is driven by the disruption of the bioenergetic function and is independent from increased ROS production. The decreased energy production in the hypertrophic growth response has been shown to lead to disturbances of intracellular calcium handling, mitochondria calcium overload and reappearance of fetal isoforms of some ATPases involved in contractile function (38).

Another study compared the mitochondrial protein profiles in the LV of spontaneously hypertensive rats (SHR) and age matched normotensive Wistar Kyoto (WKY) rats at age of 4 and 20 weeks (39). The bioenergetic pathways contributing to energy metabolism, including the fatty acid-oxidation (FAO), pyruvate oxidation, tricarboxylic acid (TCA) cycle and the common final pathway and ETC oxidative phosphorylation were analyzed in both populations. Indeed, the defects in any of these steps might disturb ATP production and impair the cardiac myocytes by inducing mitochondrial calcium overload and excess ROS (39). The defects of FAO enzymes including Cpt 2 and mitochondrial trifunctional protein subunits were previously reported in pressure overloaded hypertrophic hearts and HF (40,41). Deregulation of FAO enzymes resulted in attenuated long chain fatty acid consumption and decreased production of NADH and FADH2, leading to accumulated lipid intermediates from long chain fatty acids (LCFA) oxidation which caused cellular lipotoxicity, dissipation of mitochondria membrane potential, impairment of calcium uptake and enhancement of ROS production (39). In this study, a set of mitochondrial enzymes involved in mitochondrial metabolism pathways were found to be significantly modified in the hypertrophic LV of SHR before hypertension development. In contrast to the attenuation of enzymes involved in LCFA oxidation, the protein expression of enoyl-CoA hydratase involved in short chain fatty acids oxidation was found increased in 4-week-old SHR, probably as a compensation for the LCFA oxidation dysfunction. Under cardiac hypertrophy, fuel shifts have been demonstrated from FAO toward glucose oxidation and the key glycolytic enzyme alpha-enolase was found increased in SHR compared with age matched WKY rats. Moreover, a dysfunction of the pyruvate dehydrogenase complex (PDC) was found in

LV of SHR with a consequent reduction of the total output of NADH and of acetyl CoA from pyruvate oxidation. Since acetyl CoA produced from FAO and pyruvate oxidation is ultimately oxidized to CO2 and H_2O via the TCA cycle, its reduction results in a slowing down of this process. Moreover, several ATP synthase subunits were significantly reduced in SHR at 4 weeks, confirming the deprivation of ATP production in the early stage of LVH in SHR (39).

Ndufc2, another subunit of the CI, plays a key role in the assembly and activity of the complex (42). Different studies have investigated the characteristics of the derangements in mitochondrial structure and function consequent to Ndufc2 deficiency.

Ultrastructural damage has been detected in fibroblasts from a Ndufc2 heterozygous KO rat model (43). By performing in vitro Ndufc2 silencing in a murine vascular cell line, it has been demonstrated that Ndufc2 is a fundamental component of NADH dehydrogenase to allow regular CI assembly and activity. In fact, its downregulation led to a decreased CI integrity and function, decreased mitochondrial membrane potential and ATP production, enhanced ROS accumulation, and inflammation. Consequently, cell viability decreased whereas necrosis significantly increased. To study the function and structure of mitochondria in cells deficient for the Ndufc2 subunit of CI, primary skin fibroblasts from heterozygous stroke resistant SHR (SHRSR)_KO for Ndufc2 gene and control SHRSR_wild type (WT) were cultured. The intracellular levels of ROS were compared in either unstimulated or high-NaCl treated primary cultures. Under basal experimental conditions the amount of actively respiring mitochondria, membrane potential, the mitochondrial depolarization index and the percentage of cells with a low mitochondrial

membrane potential were similar among the two cell lines. Conversely, SHRSR_KO Ndufc2 fibroblasts showed a time-dependent reduction of mitochondrial membrane potential and mitochondrial depolarization index which reached the lowest peak at 72 hours in response to high-NaCl medium compared with SHRSR_WT fibroblasts. To assess whether the mitochondrial dysfunction observed in the SHRSR_KO Ndufc2 fibroblasts could be related to the generation of increased oxidative stress, intracellular ROS levels were observed by cytofluorimetric analysis. At baseline and during the time-course exposure to high-NaCl medium, the SHRSR_KO Ndufc2 cells generated greater amounts of intracellular and mitochondrial ROS than those produced from the SHRSR_WT fibroblasts. Ndufc2 deficiency is also responsible of structural alterations in mitochondrial membrane system (43). Two parameters of ultrastructural degeneration were considered, namely the percentage of mitochondrial area carrying intact cristae and the loss of inner mitochondrial membrane (IMM) assessed as the IMM/OMM (outer MM) index. At baseline, the amount of mitochondria with normal ultrastructure or with slight damage was similar among cultures, whereas a moderate damage was observed in 35% and 15% (ratio 2.3) of the mitochondrial population of the SHRSR_KO Ndufc2 and SHRSR_WT fibroblasts, respectively, and severe damage category was observed only in the mitochondrial population of SHRSR_KO Ndufc2 cells. The overall damage was observed in 70% of SHRSR_KO Ndufc2 compared with 45% of SHRSR_WT fibroblasts, with a significant total ratio of 1.55. After 72 hours of high-NaCl exposure, the SHRSR_WT fibroblasts showed no significant changes of mitochondrial damage score while mitochondrial damage was enhanced in SHRSR_KO-Ndufc2 cells with an overall amount of 85% (43).

Moreover, SHRSR_WT fibroblasts showed higher IMM/OMM index values, with minimal and no significant changes after high-NaCl exposure, which reflected the preservation of the integrity of mitochondria ultrastructure even after stimulation. Treatment with resveratrol, a natural molecule with anti-inflammatory and antioxidant actions able to inhibit ROS generation, dampened the mitochondrial depolarization, the mitochondrial oxidative stress and the mitochondrial morphological damage observed after high-NaCl exposure in SHRSR_KO, suggesting a direct involvement of ROS production in the onset of mitochondrial dysfunction and mitochondrial morphology impairment (43).

In vivo, a heterozygous Ndufc2_KO rat model, obtained from the parental SHRSR strain, showed a deficient CI assembly and, once fed with high-salt/low potassium Japanese-style diet, developed renal damage followed by stroke occurrence, resembling the stroke prone SHR (SHRSP). In addition, a higher grade of cardiac hypertrophy was detected in SHRSR_KO (44).

Likewise, the association of the T allele of rs11237379 (belonging to the human gene) with a significantly reduced *NDUFC*2 expression and with increased risk of early-onset ischemic stroke supports the hypothesis that reduced *NDUFC*2 expression could contribute to increased stroke susceptibility also in humans. The pathogenic relevance of the rs11237379 allele variant was enhanced by the concomitant presence of a second allele variant at rs641836 (44).

The effects of Ndufc2 on oxidative stress and mitochondrial damage were also confirmed in mitochondria from peripheral blood mononuclear cells (PBMCs) from subjects carrying the gene variant (T allele of rs11237379) associated with decreased *NDUFC*2 expression compared to those carrying

the wild type allele (C allele). At baseline the burden of overall mitochondrial damage was similar among TC and CC subject PBMCs whereas PBMCs from TT subjects showed an overall damage significantly higher with respect to PBMCs from both TC and CC subjects. The high-NaCl exposure produced a strong increase in mitochondrial damage in the PBMCs from TT subjects. Of note, PBMCs from TC and CC carriers showed a slight and not significant increase of mitochondrial overall damage, as compared with baseline conditions in the absence of stimulus. These findings were corroborated by the IMM/OMM index analysis. A slight no significant reduction of the IMM/OMM values was observed in PMBCs from TC and CC subjects after exposure to high-NaCl. Finally, the standardized stimulation with LPS produced effects like those observed with high-NaCl stimulation in all PBMCs cultures (43).

To evaluate whether the treatment with ROS scavengers could affect the alterations of mitochondrial parameters also in human PBMCs, cells from TT and CC subjects were pretreated before the salt stimulation with resveratrol. As expected, the PBMCs from CC subjects did not show any change of all mitochondrial parameters. In contrast, similarly to the in vitro rat model, resveratrol was able to exert a strong scavenging effect on ROS generation, to counteract the mitochondrial membrane depolarization and the overall burden of ultrastructural damage induced by the high-NaCl stimulation. These results clearly indicated that a decreased *NDUFC*2 expression related to T/C rs11237379 gene variant determined a status of mitochondrial dysfunction and of increased oxidative stress, which was associated with ultrastructural impairment of mitochondrial morphology, similarly to what was observed in primary fibroblasts from the Ndufc2 heterozygous KO rat model. In both models, the mitochondrial damage was

exacerbated by high-NaCl exposure and counteracted by the scavenging of intracellular ROS. Moreover, TT and TC had markedly reduced KCT21 and proliferator-activated receptor gamma coactivator 1α (PGC-1α) expression compared with CC/rs11237379 subjects, suggesting a potential synergistic role between Ndufc2/CI dysfunction and dysregulation of PGC-1α mediated mitochondrial biogenesis (43).

1.c The role of sirtuins in the development of LVH

Mammalian sirtuins (SIRT) are NAD+-dependent deacylases with a huge range of roles in transcription regulation, energy metabolism modulation, cell survival, DNA repair, inflammation, and circadian rhythm regulation (45-47). SIRT1 is found in the nucleus and cytosol and, along with histone deacetylation, also modulates transcription factors such as p5319, nuclear factor kappa-light-chain-enhancer of activated B cells (NF-κB), class O of forkhead box transcription factors (FOXOs), PGC-1α and DNA repair proteins such as Poly ADP-ribose polymerase 1 (PARP1) (48,49). SIRT2 is a cytosolic SIRT, while SIRT3, 4, and 5 are in the mitochondria and have roles in oxidative stress and lipid metabolism. SIRT6 and 7 are nuclear sirtuins exerting a role in gene expression and DNA repair (50).

Regarding mitochondrial function, SIRT1 and SIRT3 have been described as critical components in maintaining mitochondria homeostasis (51-64).

The deletion of either SIRT1 or SIRT3 in experimental models of young (4–6 months) mice produced impairment of cardiomyocyte contractility and ageing-like cardiac dysfunction upon stress conditions, indicating the crucial role of SIRT1 and SIRT3 in protecting myocardial contractility from oxidative stress injury (65). The deficiency of SIRT1/SIRT3 led to the inactivation of adenosine monophosphate (AMP)-activated protein kinase (AMPK) and alterations in OXPHOS that causes impaired mitochondrial

respiration (52,53,58,63). Moreover, SIRT1 deacetylates mitofusin 1 (MFN1) and mitofusion 2 (MFN2), which contribute to the mitochondria elongation under hypoxic condition (66,67). SIRT3 can directly deacetylate optic atrophy 1 (OPA1) to increase mitochondrial fusion levels (55,62). Deacetylation of FOXO3 by SIRT3 can promote MFN2 expression, thus repairing the imbalance of mitochondrial fission and fusion and maintaining mitochondrial function (57,61). Both SIRT1 and SIRT3 play an important role in regulating the activation of AMPK, which is a critical factor to protect cardiomyocyte mitochondrial function. Indeed, the deficiency of SIRT1 and SIRT3 resulted in a marked reduction of phosphorylation levels of AMPK during oxidative stress conditions. Cardiac SIRT1 and SIRT3 defects were responsible of an impaired cardiac function since AMPK plays an important role in the regulation of myocardial signaling and contractile function. SIRT3 deficiency might upregulate mitochondrial calcium uniporter (MCU) expression involved in AMPK regulation that accounts for exaggerated MCU-mediated mitochondrial calcium uptake and results in the elevated calcium flux during cardiomyocyte contraction (52,53,58,63).

In addition, a decline in OXPHOS Complex subunits was observed in case of deletion of SIRT3, and the response to oxidative stress of the subunits of CI to Complex V was significantly impaired.

Moreover, the mitochondrial DNA (mtDNA) content was decreased in SIRT1 and SIRT3 deficient hearts along with increased mtDNA damage occurrence. A deficiency of SIRT1 and SIRT3 has been also demonstrated to cause mitochondrial structural alterations of cellular cultures of cardiomyocytes, consisting of significantly impaired cristae structure with brighter and diminished cristae membrane surface area. Interestingly,

mitochondria had a larger network with longer branches suggesting the imbalanced mitochondria fission and fusion (68).

SIRT are also responsible of the deacetylation of NAD+ by removing an acetyl group from target substrates via the conversion of NAD+ to nicotinamide (NAM) and O-acetyl-ADP-ribose. Loss of SIRT activity and reduction of NAD+ levels are implicated in the etiology of different cardiovascular diseases including atherosclerosis, hypertrophy and HF (46,47). Conversely, SIRT1 overexpression protected against hypertrophy, fibrosis and cardiac dysfunction in a mouse model. Cardiomyocytes with SIRT1 activation either genetically or upon resveratrol were protected against phenylephrine-and isoprotenerol-induced hypertrophy and related inflammation. Other mouse studies using either stress-induced or diabetes models of cardiomyopathy confirmed that SIRT1 KO increased hypertrophy and decreased cardiac function. The treatment with either the SIRT activator STAC-3 or resveratrol was protective (64).

SIRT3 has been also demonstrated to have a clear protective role in cardiac hypertrophy. In fact, SIRT3 knockout mice developed hypertrophy and fibrosis because of increased mitochondrial permeability transition pore (mPTP) opening and TGF-β1 signaling. SIRT3 knockout mice are also more sensitive to the hypertrophic effects of trans-aortic coarctation, ATII and isoprotenerol than wild-type mice. SIRT3 overexpression resulted in resistance to hypertrophy-inducing stimuli, because of increased FOXO3a, manganese superoxide dismutase (MnSOD), oxoguanine glycosylase (OGG), parkin and catalase activation (69). Moreover, the protective effects of resveratrol on hypertrophy and fibrosis may be a result of both SIRT1 and SIRT3 activation, since they were not observed in SIRT3 KO mice. Treatment with honokiol, a poly-phenolic compound believed to activate

SIRT3, prevented hypertrophy, fibrosis, mitochondrial damage, and cell death in mice exposed to pressure overload and drug-induced HF (70). Cardiomyocytes cultured from SIRT3-deficient hearts showed increased ROS levels, when compared with their respective wild-type controls, suggesting that SIRT3 prevented cardiac hypertrophic response by scavenging cellular ROS (71). Indeed, SIRT3 blocks cardiac hypertrophy by suppressing the AKT signaling in cardiomyocytes throughout the deacetylation and activation of LKB1 and thereby activating AMPK, which is known to suppress AKT phosphorylation (63). Moreover, SIRT3-mediated deacetylation promotes nuclear localization of FOXO3a, leading to enhanced transcription of FOXO3a-dependent antioxidant genes, such as MnSOD, thus reducing cellular ROS levels. In fact, SIRT3-deficient mice showed reduced activity of MnSOD and catalase (72). It should be also underlined that increased ROS levels are known to activate Ras, which in turn activates AKT (73). By blocking cellular ROS levels, SIRT3 shuts down the activity of Ras and thus the activity of AKT. Therefore, in case of deficiency of SIRT3 the Ras oncoprotein and its downstream targets, namely mitogen-activated protein kinase (MAPK)/ extracellular signal-regulated kinase (ERK) and phosphoinositide 3-kinases (PI3K)/AKT signaling pathways may be upregulated (73). The upregulation of the PI3K/AKT pathway produces an increased activation of mammalian target of rapamycin (mToR) which enhances cell growth, proliferation, motility, and survival, thus contributing to the development of cellular hypertrophy. On the other hand, PI3K/AKT inhibits the activation of GATA4 which is an important transcriptional regulatory factor able to counterbalance cell growth (74) (Figure3).

Figure 3. Protective action of SIRT3 against cardiac hypertrophy development

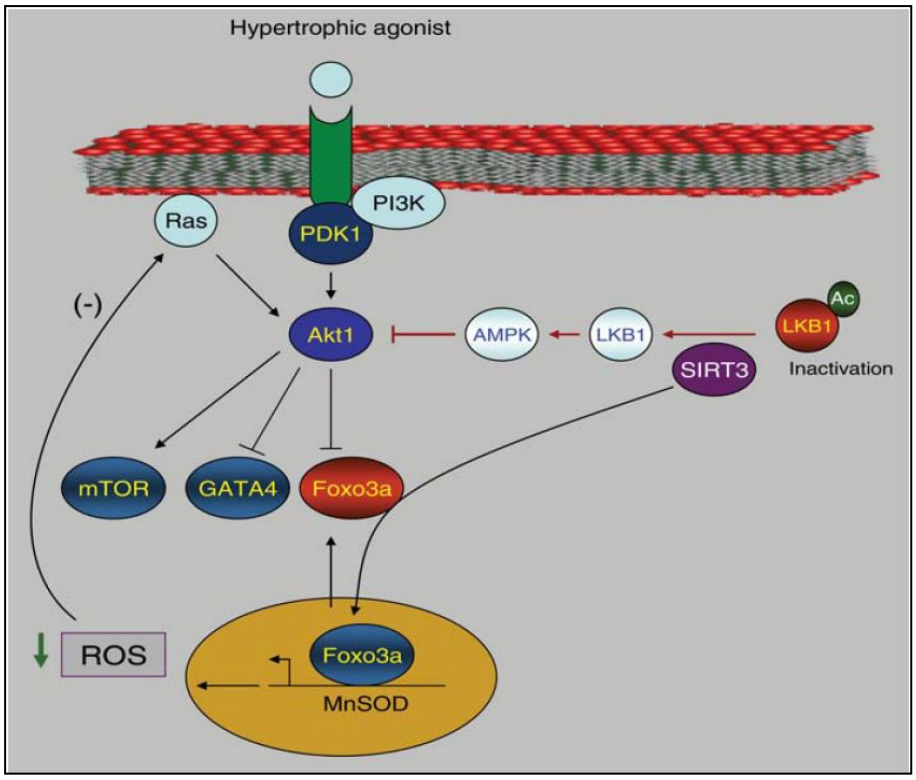

Several studies have suggested that increasing NAD+ may protect from hypertrophy by increasing energy production in the mitochondria and reducing mPTP opening. The addition of NAD+ prevented isoproterenol-induced hypertrophy in mice and interestingly this was mediated by SIRT3, but not SIRT1, through activation of LKB1-AMPK signaling (63). Consistently, PARP inhibitors protected against hypertrophy and improved cardiac function in several rodent models, probably in part by increasing NAD+ levels (75).

Overall, both increasing SIRT3 activity and boosting NAD+ levels appear to be promising approaches to protect against hypertrophy and fibrosis.

2. Aims of the study

We examined the role of Ndufc2 deficiency and of subsequent CI dysfunction on the development of cardiac hypertrophy both in an in-vitro model and in humans.

The principal aims of the in vitro studies were:

- To determine if Ndufc2 deficiency (achieved by gene silencing) is associated with cell hypertrophy in cardiomyocytes (supported by the expression of atrial natriuretic peptide and β-myosin heavy chain and by fluorescence analysis for α-actin) and to investigate the involved molecular mechanisms (by analyzing the genetic and protein expression of: SIRT3, FOXO3a, MnSOD, AMPK, phosphoAMPK, AKT-1, phospho-AKT-1, mTOR).
- To evaluate if NAD+ supplement can induce the regression of cardiac hypertrophy, through the reactivation of CI, in Ndufc2 silenced cells.

The principal aims of the human study were:

- To assess whether hypertensive subjects carrying the A mutant allele at rs641836 and the T mutant allele at rs11237379 of *NDUFC2* show a higher degree of cardiac hypertrophy compared to individuals carrying the G and the C wild type allele, respectively, for each marker.

3. In vitro study: Methods

3.1.a Ndufc2 gene silencing in H9c2 commercially available cardiomyocytes

Commercially available H9c2 cardiomyocytes were cultured in DMEM containing normal glucose (5.5 mmol/L), 10% FBS, and supplemented with

penicillin (100 U/mL)/streptomycin (100 lg/mL) at 37°C in 95% O2 and 5% CO2. Cells were plated in 100-mm-diameter dishes (49105) and 60-mm-diameter dishes (1.59105), passaged upon reaching confluence with 2 mL of trypsin and used at the 12th passage and 70% confluence. Cells were washed with PBS, and then OPTI-MEM–reduced serum medium (Invitrogen, Carlsbad, CA) was added to the cells. Ndufc2-specific siRNA (Mission siRNA; Sigma-Aldrich) and a nucleic acid transferring agent, Lipofectamine 2000 (Invitrogen) were incubated in OPTI-MEM–reduced serum medium for 20 minutes at RT to form a siRNA-Lipofectamine complex. The siRNA-Lipofectamine complex-containing medium was added to cells to a final siRNA concentration of 33 nmol/L. Five hours later, the complex-containing medium was replaced with DMEM supplemented with 10% FBS. Cells transfected with Lipofectamine and no-target siRNA (Sigma-Aldrich) were used as controls. Seventy-two hours later, both silenced and non-silenced cells were used for all analyses described below. Six experiments were performed.

3.1.b Determination of atrial natriuretic peptide and β-myosin expression by Reverse-Transcription Polymerase Chain Reaction in cellular RNA extracts

Two micrograms of total RNA were used for cDNA synthesis using Superscript III First-Strand (Invitrogen, Carlsbad, CA) and random examer primers according to manufacturer's instructions. The following oligonucleotides were used:

ANP: forward CTGGGACCCCTCCGATAGAT; reverse TTCGGTACCGGAAGCTGTTG; ß-miosin: forward ATGTGCCGGACCTTGGAAG; reverse CCTCGGGTTAGCTGAGAGATCA; ß-actin: forward 50-

AGATGACCCAGATCATGTTTGAGA-30; reverse 50-ATAGGGACATGCGG AGACCG-30. All RNA samples were adjusted to yield equal amplification of hypoxanthine-guanine phosphoribosyl transferase as an initial standard: forward TGAGGCCGGTGCTGAGTATGTCG; backward CCACAGTCTTCTGGGTGGCAGTG. Real-time quantitative polymerase chain reaction. (RT-PCR) was performed using a 29 SYBR Green PCR Master Mix (Applied Biosystems, Forster City, CA) containing the double-stranded DNA-binding fluorescent probe, Sybr Green, and all necessary components except primers. Quantitative PCR conditions included an initial denaturation step of 94°C/10 minutes followed by 40 cycles of 94°C/15 seconds and 60°C/15 seconds. Standards, samples, and negative controls (no-template) were analyzed in triplicate. Concentrations of mRNA were calculated from serially diluted standard curves simultaneously amplified with the unknown samples and corrected for b-actin mRNA levels. Levels of ANP and ß-miosin mRNA in Ndufc2-silenced cells were compared to those of non-silenced cells.

3.1.c Western blotting of total proteins extracted from H9c2 Ndufc2-silenced cardiomyocytes and controls

Cells were washed twice with ice-cold PBS and lysed with lysis buffer. Protein concentrations were determined by the Bradford method. Then, 40 μg of total proteins were separated on 12% SDSPAGE and transferred to polyvinylidene difluoride (PVDF) membranes (Amersham, Piscataway, NJ). Nonspecific binding sites were blocked with 5% nonfat dried milk for 2 hours at room temperature. Membranes were then incubated overnight with the following primary antibodies: anti-SIRT3; anti- FOXO3a, anti-MnSOD, anti-AMPK, anti-phosphoAMPK, anti-AKT-1, anti-phospho-

AKT-1, anti-P-S6K (ribosomal protein S6 kinase beta-1 [P-6SK], used as a hallmark of activation by mTOR).

Signals were revealed with an enhanced chemiluminescence detection system (ECL; Amersham) and visualized by a ChemiDoc XRS+imaging system (Bio-Rad, Richmond, CA). Finally, protein levels were normalized using b-actin, VINC or Glyceraldehyde 3-Phosphate Dehydrogenase (GPDH) levels. Protein bands were scanned and quantified densitometrically throughout ChemiDoc XRS+imaging.

3.1.d Cell hypertrophy detected with fluorescence microscopy

Cell hypertrophy was assessed in H9c2 silenced for Ndufc2 for 48 hours. Cells were plated in 24 multiwell, fixed with 4% paraformaldehyde for 15 min, washed with PBS three times and blocked in 5% bovine serum albumin, 5% goat serum in PBS for 30 min. Then, cells were subjected to immunofluorescence protocol using a mouse monoclonal anti- β-actin (Santa Cruz, sc-69879). For detection in fluorescence, a secondary goat anti-mouse Alex Fluor 488 was used. Cell nuclei were counterstained with 0.1 mg/mL Höechst (Invitrogen, Carlsbad, CA, Cat. H3570) and images were acquired by an inverted microscope. Cell size was quantified in randomly chosen fields by Image J (National Institutes of Health, USA).

3.2.Cell culture of rat primary cardiomyocytes

Neonatal rat ventricle cardiomyocytes (CMs) were isolated from 1-2 days neonatal WKT rats through an enzymatic digestion followed by a magnetic separation, by using the Miltenyi technology (Miltenyi Biotec, Bergisch Gladbach, Germany). CMs were cultured as previously described (76).

3.2.a Western blotting of total proteins extracted from Ndufc2-silenced rat primary cardiomyocytes and controls

Cells were washed twice with ice-cold PBS and lysed with lysis buffer. Protein concentrations were determined by the Bradford method. Then, 40 μg of total proteins were separated on 12% SDSPAGE and transferred to polyvinylidene difluoride (PVDF) membranes (Amersham, Piscataway, NJ). Nonspecific binding sites were blocked with 5% nonfat dried milk for 2 hours at room temperature (RT). Membranes were then incubated overnight with the primary antibody anti-SIRT3.

Signals were revealed with an enhanced chemiluminescence detection system (ECL; Amersham) and visualized by a ChemiDoc XRS+imaging system (Bio-Rad, Richmond, CA). Finally, protein levels were normalized using vinculin. Protein bands were scanned and quantified densitometrically throughout ChemiDoc XRS+imaging.

3.2.b Hypertrophy of rat primary cardiomyocytes detected with fluorescence microscopy

Cell hypertrophy was assessed in CMs silenced for Ndufc2 for 48 hours. Cells were plated in 24 multiwell, fixed with 4% paraformaldehyde for 15 min, washed with PBS three times and blocked in 5% bovine serum albumin, 5% goat serum in PBS for 30 min. Then, cells were subjected to immunofluorescence protocol using a mouse monoclonal anti- β-actin (Santa Cruz, sc-69879). For detection in fluorescence, a secondary goat anti-mouse Alex Fluor 488 was used. Cell nuclei were counterstained with 0.1 mg/mL Höechst (Invitrogen, Carlsbad, CA, Cat. H3570) and images were acquired by an inverted microscope. Cell size was quantified in randomly chosen fields by Image J (National Institutes of Health, USA).

4. Human study: Methods

4.a Study population

Two thousand and thirty-two unrelated Caucasian adults who were referred to the Department of Cardiology, Sapienza University, Sant'Andrea Hospital, Rome, for hypertension management were enrolled in this study.

Hypertension was diagnosed on the basis of the presence of office systolic blood pressure (SBP) values >=140 mmHg and/or diastolic BP (DBP) values >=90 mmHg (average of 3 repeated measurements made by the same doctor with a mercury sphygmomanometer). Also subjects who self-reported treatment with antihypertensive drugs, namely ACE inhibitors (ACEi), angiotensin receptor blockers (ARB), calcium channel blockers (CCB), thiazide/thiazide-like diuretics, loop diuretics, mineralocorticoid receptor antagonists (MRA), beta-blockers and alpha-blockers, were considered hypertensives.

Subjects with cardiomyopathies or valvular diseases (e.g. aortic stenosis) potentially causing LVH were excluded. Only patients with normal LV function without wall motion abnormalities were included.

Physical examination, blood pressure measurement, electrocardiogram (ECG) and echocardiogram were performed in all patients.

The presence of hypercholesterolemia, diabetes mellitus, and smoking habit and pharmacological treatment were recorded.

4.b Electrocardiogram

A 12-lead ECG was performed in all hypertensive patients. The ECG is not a particularly sensitive method for detecting LVH and its sensitivity varies according to body weight.

According to 2018 European Society of Cardiology/ European Society of Hypertension (ESC/ESH) Guidelines, ECG LVH has been defined based on the most commonly used criteria:

- SV1+RV5 (Sokolow–Lyon criterion) >35 mm
- R wave in aVL >=11 mm
- SV3+RaVL (Cornell voltage) >28 mm (men) >20 mm (women)
- Cornell duration product >2440 mm*ms

4.c Transthoracic echocardiography

Since the ECG cannot exclude LVH because of poor sensitivity, all patients underwent mono-dimensional and bi-dimensional transthoracic echocardiography.

Two-dimensional transthoracic echocardiography (TTE) provides information about LV geometry, left atrial volume, aortic root dimensions, LV systolic and diastolic function, pump performance, and output impedance.

LV internal diameters, septal thickness, and posterior wall thickness were measured according to the guidelines of the American Society of Echocardiography and European Association of Cardiovascular Imaging (77). The LV mass was calculated at end diastole by applying the Devereux correction to the American Society of Echocardiography cube LV mass formula. The relative wall thickening (RWT) was calculated as: 2 * posterior wall thickness divided by LV diastolic diameter or, septal wall thickness + posterior wall thickness divided by LV diastolic diameter.

Abnormal LV geometry in hypertensive patients is frequently associated with diastolic dysfunction which can be further evaluated by a combination of transmitral flow and tissue Doppler studies. Left atrial (LA) size is also

frequently increased in hypertensive patients and is related to diastolic dysfunction.

The recommended parameters for the definition of LVH by echocardiography are:

- LV mass/height$^{2.7}$ (g/m$^{2.7}$) >50 (men) >47 (women)
- LV mass/body surface area (BSA) (g/m^2) >115 (men) >95 (women)
- LV concentric geometry RWT >=0.43
- LA volume/height^2 (mL/m2) >18.5 (men) >16.5 (women)

4.d Genomic DNA extraction

Genomic DNA was isolated from venous peripheral blood by using the FlexiGene kit (Qiagen). Quality and concentration of DNA were determined by a NanoDrop1000 spectrophotometer (Thermo Fisher Scientific).

4.e Genotyping

We studied 2 tag SNPs in *NDUFC*2: rs641836 and rs11237379 by 7900HT real-time PCR and TaqMan technology assays (c__26529993_10 and c__2999825_10, respectively; Life Technologies). The two *NDUFC*2 tag SNPs were selected for analysis by using the algorithm-Taggerpairwise Tagging (HapMap database and software, http:// hapmap.ncbi.nlm.nih.gov) on *NDUFC*2 gene for CEU population.

Polymorphism's information was assessed in the Single Nucleotide Polymorphism (dbSNP) NCBI (http://www.ncbi. nlm.nih.gov/entrez/query.fcgi?db=snp&cmd=search&term=), and ENSEMBL (http://www.ensembl.org/index.html) databases.

Real-time polymerase chain reaction (RT-PCR) of human *NDUFC*2 was performed with the following set of oligonucleotides: forward 50-CCTGTATGCTGTGAGGGACC-30 and reverse 50-

CGACGTTCAGCTCCACAACA-30. b-actin: forward 50-GCAAGAGATGGCCACGGCTG-30 and reverse 50-CCAC AGGACTCCATGCCCAG-30.

5. Statistical analysis

Statistical analysis was performed using the SPSS version 25 (SPSS Inc., Chicago, Illinois).

In the *in vitro* studies data of RNA levels, Western blot densitometric analyses and results of fluorescence-activated cell sorting are provided as means and standard deviation (SD). Differences between groups (Ndufc2-silenced H9c2 or CMs and respective controls) were analyzed by t test.

In the human study categorical variables are expressed as frequencies and percentages. Continuous data are given as mean value and SD.

Differences between groups were analyzed either by t test or 1-way analysis of variance (ANOVA) if groups were more than two. The Bonferroni post-hoc least significant difference test was performed to complete the analysis for multiple comparisons. A covaried 1-way ANOVA was performed considering each cardiac parameter as a dependent variable; considering age, gender, body mass index (BMI), office BP, antihypertensive treatment with a combination of two or more drugs and the number of BP-lowering agents as covariates; and considering the polymorphism showing significant differences in the analyses among groups as an independent value.

Deviation from the Hardy-Weinberg equilibrium was analyzed with the chi-square test. A value of $P<0.05$ was chosen as the cut-off level for statistical significance.

6. In vitro results

6.a H9c2 silenced cells

Cellular hypertrophy in the Ndufc2-silenced cells was documented by fluorescence microscopy for the α-actin and by gene expression analysis of the ANP and β-myosin heavy chain. RNA and proteins were extracted from silenced and not silenced cells and used for the assessment of the SIRT molecular pathway. We found that Ndufc2-silenced cardiomyocytes, compared to not silenced cells, showed a significant degree of hypertrophy by fluorescence microscopy ($p<0.01$) (Figure 4, Panel A), with a significant increase of both hypertrophy markers ($p<0.01$) (Figure 4, Panel B).

Figure 4. Cell hypertrophy development after Ndufc2 gene silencing in H9c2.

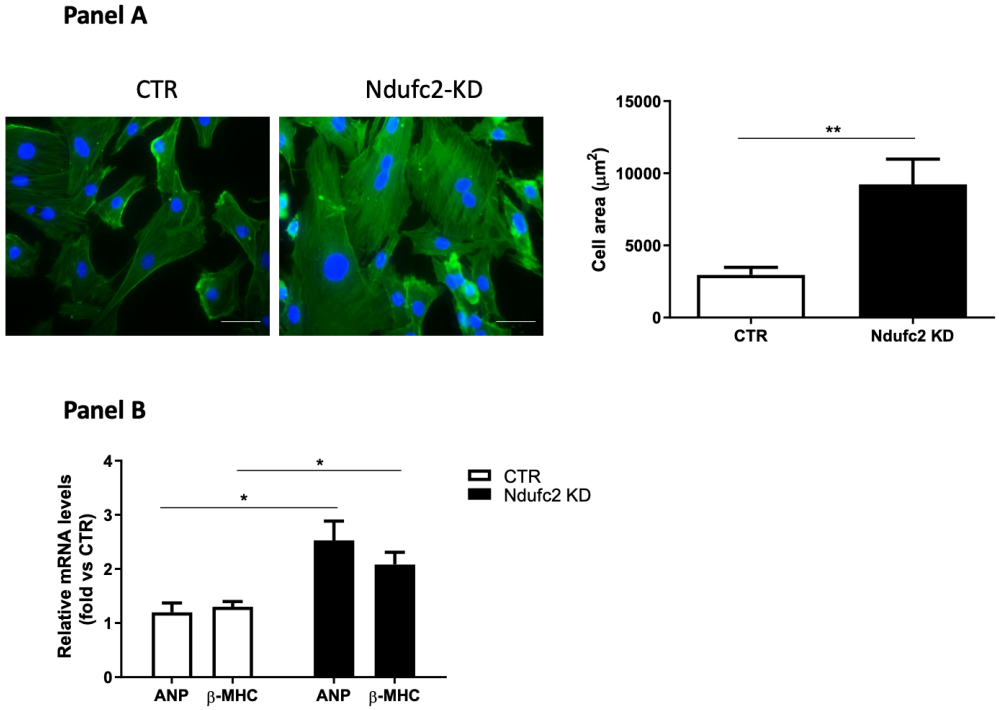

In parallel, SIRT3 (Figure 5, Panel A) and its downstream molecules (FOXO3a [Figure 5, Panel B], MnSOD [Figure 5, Panel C], phospho-AMPK,[Figure 5, Panel D]) were significantly reduced ($p<0.05$), with an

increase of phospho-AKT (Figure 5, panel E) and of P-6SK as a marker of the mTOR pathway ($p<0.05$) (Figure 5, panel F).

Figure 5. Effects of Ndufc2-silencing on SIRT3 associated molecular pathways

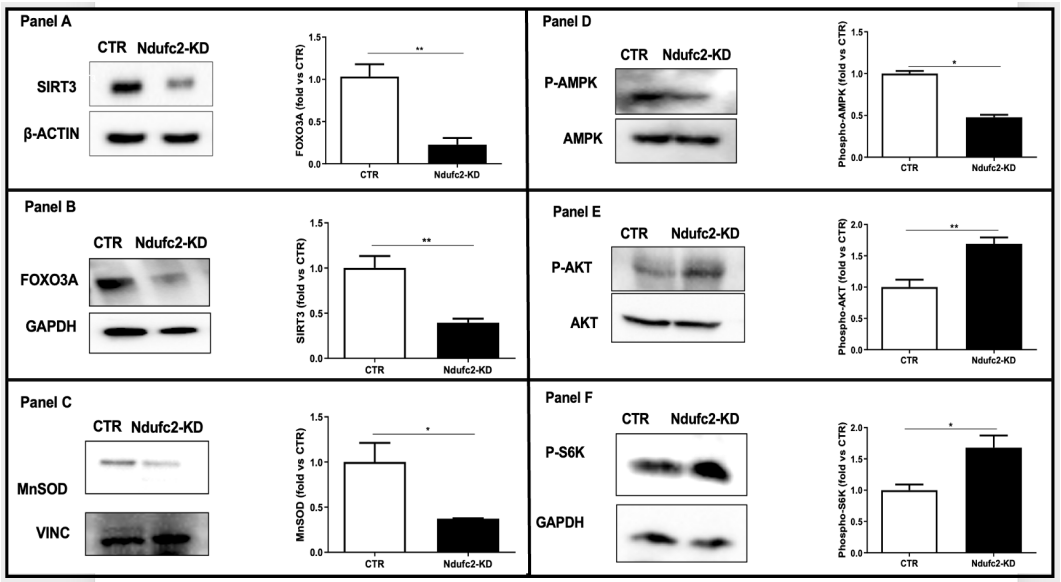

Ndufc2-deleted cardiomyocytes were then exposed to NMN 1 μM to evaluate the impact of NAD+ supplementation on cardiac hypertrophy. In fact, the administration of NMN was able to reduce the cellular volume (Figure 6, Panel A) and the gene expression level of both hypertrophy markers (Figure 6, Panel B).

Figure 6. NMN supplementation rescues cell hypertrophy induced by Ndufc2 deficiency

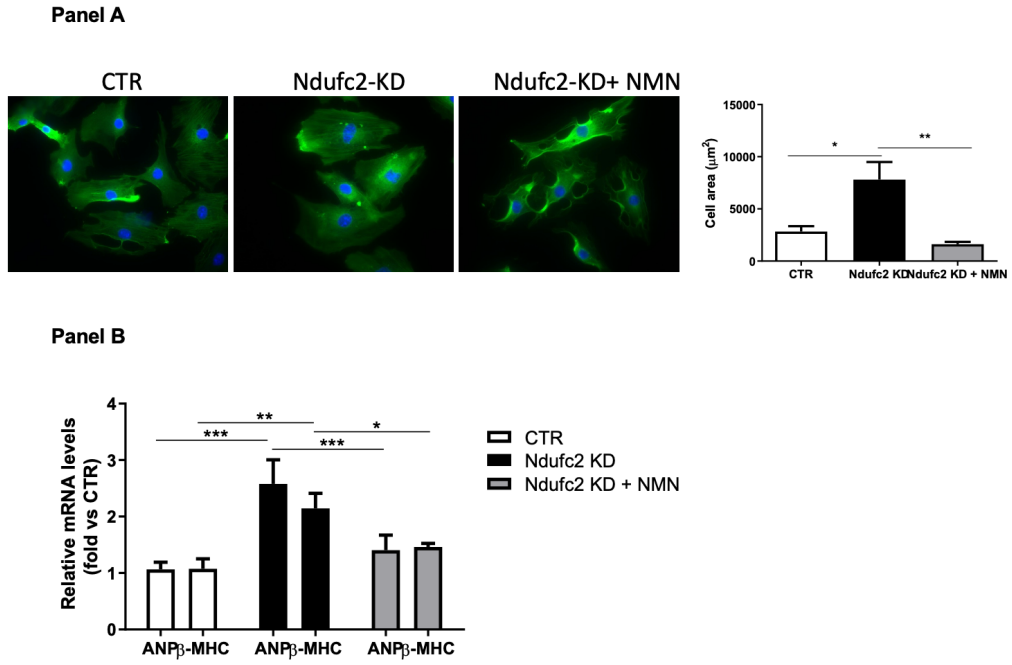

6.b Rat primary cardiomyocytes

After Ndufc2-silencing, rat neonatal cardiomyocytes developed a significant higher degree of hypertrophy, as detected by fluorescence microscopy ($p<0.05$) (Figure 7, Panel A). SIRT3 levels were significantly reduced as detected by Western blot analysis compared to control ($p<0.05$) (Figure 7, Panel B). After NMN supplementation the cellular area was significantly reduced at fluorescence microscopy ($p<0.05$) (Figure 7, Panel C).

Figure 7. Cell hypertrophy and reduced expression of SIRT3 in Ndufc2 gene silenced rat neonatal cardiomyocytes

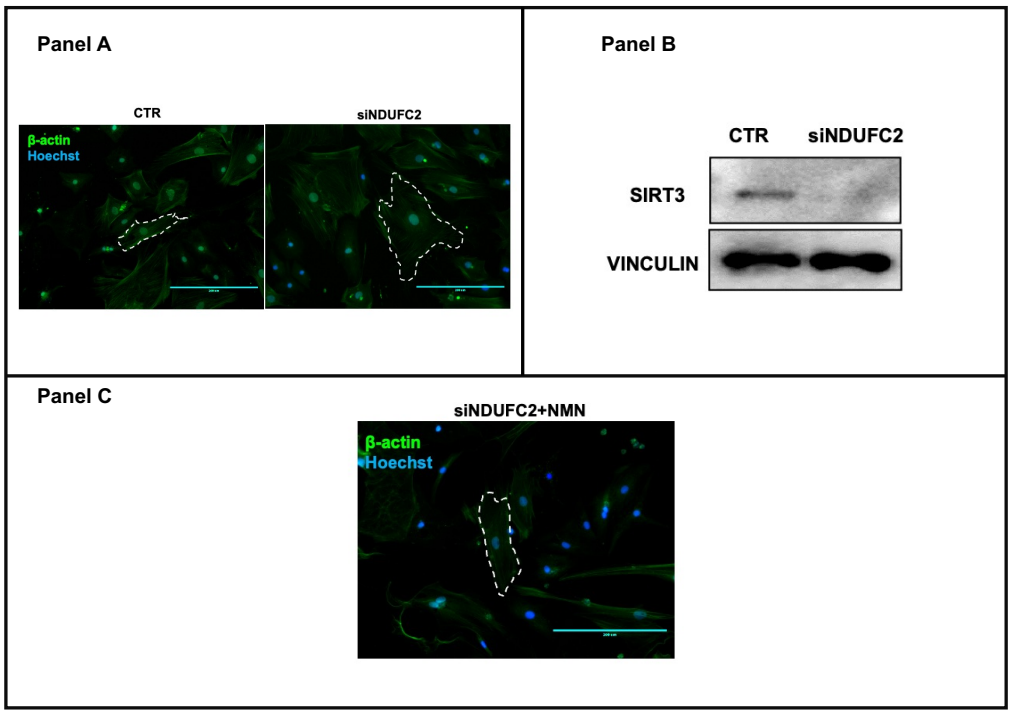

7. Human study results

The population of the present study included 232 hypertensive subjects (136 male, 58.6%) with a mean age of 59 ± 15 years. Main anthropometric, clinical, echocardiographic and pharmacological variables are reported in Table 1.

Table 1. Characteristics of the overall population (n=232)

General data	
Age, years	59 ± 15
Male sex, n (%)	136 (58.6)
BMI, Kg/m2	25.7 ± 3.6

Diabetes, n (%)	41 (17.6)
Dyslipidaemia, n (%)	95 (41)
Clinic SBP, mmHg	145.6 ± 16.9
Clinic DBP, mmHg	87.1 ± 9.8
24h mean SBP, mmHg	129.1 ± 13.1
24h mean DBP, mmHg	78.1 ± 8.9
Echocardiographic data	
Septal thickness, mm	10.1±1.6
LVPW, mm	9.8±1.6
RWT	0.41±0.06
LVEDd, mm	48.6±4.1
LV mass, g	172.1±47.9
LV mass/BSA, g/m2	93.2±23.8
LV mass/$h^{2,7}$, g/$m^{2,7}$	39.6±13.1
LA vol/h^2, ml/m^2	15.3±3.4
LVEF, %	67.5±9.7
Pharmacological therapy	
ACEi, n (%)	43 (18.6)
ARB, n (%)	104 (45)
Calcium channel blockers, n (%)	87 (37.7)
Thiazide diuretics, n (%)	60 (26)

Beta-blockers, n (%)	52 (22.5)
MRA, n (%)	10 (4.3)
Combination therapy, n (%)	118 (51)
2 drugs, n (%)	83 (35.6)
3 drugs, n (%)	25 (11)
4 drugs, n (%)	10 (4.5)

Legend to Table 1

ACEi, angiotensin converting enzyme inhibitors; ARB, angiotensin receptor blockers; BMI, body mass index; DBP, diastolic blood pressure; LA, left atrium; LV, left ventricle; LVEDd, left ventricular end-diastolic diameter; LVEF, left ventricular ejection fraction; LVPW, left ventricular posterior wall; MRA, mineracolorticoid receptor antagonists; RWT, relative wall thickening; SBP, systolic blood pressure.

Seventy-five individuals (32%) presented LVH according to 2018 European Guidelines echocardiographic criteria. Beside echocardiographic parameters and treatment with ACEi, patients with and without LVH had comparable characteristics (Table 2).

Table 2. Characteristics of the population according to LVH

General data	**With LVH (n=75)**	**Without LVH (n=157)**	**p-value**
Age, years	60±15	58±14	NS
Male sex, n (%)	45(60)	91 (56)	NS
BMI, Kg/m2	25.2±3.3	26.1±3.6	NS
Diabetes, n (%)	12 (16)	29 (18)	NS

Dyslipidaemia, n (%)	31 (41)	60 (38)	NS
Clinic SBP, mmHg	146±18	144±17	NS
Clinic DBP, mmHg	87±10	87±9	NS
24h mean SBP, mmHg	131±12	130±14	NS
24h mean DBP, mmHg	77±9	79±9	NS
Echocardiographic data			
IVSd, mm	11.2±1.6	9.5±1.1	<0.001
LVPWd, m	11.1±1.5	9±1.2	<0.001
RWT	0.45±0.07	0.38±0.05	<0.001
LVEDd, mm	50±4	48±4	0.011
LV mass, g	206.9±48.3	150.6±32.7	<0.001
LV mass/BSA, g/m2	113.8±22.9	80.6±13.4	<0.001
LV mass/$h^{2,7}$, $g/m^{2,7}$	50.5±10	33.2±10	<0.001
LA vol/h2, ml/m2	18.6±4.1	14.0±2.0	<0.001
LVEF, %	69±10	68±10	NS
Pharmacological therapy			
ACEi, n (%)	10 (13)	33 (21)	0.032
ARB, n (%)	36 (48)	68 (43)	NS
Calcium channel blockers, n (%)	30 (39)	57 (36)	NS
HCTZ, n (%)	17 (23)	43 (27)	NS

Beta-blockers, n (%)	14 (19)	38 (24)	NS
MRA, n (%)	2 (3)	8 (5)	NS
Combination therapy, n (%)	33 (48)	69 (53)	NS

For abbreviations see Table 1.

With regard to the allele frequencies and chi-square test results for Hardy-Weinberg equilibrium for each genotype:

- *NDUFC2* rs641836 polymorphism: 79.7% for the G allele and 20.3% for the A allele (Figure 8, Panel A); 62.9% for GG genotype, 33.7% for GA genotype and 3.4% for AA genotype (Figure 8, Panel B); chi-square test: $p > 0.05$;
- *NDUFC2* rs11237379 polymorphism: 43.3% for the C allele and 56.7% for the T allele (Figure 9, Panel A); 16.7% for CC genotype, 53.3% for CT genotype and 30% for TT genotype (Figure 9, Panel B); chi-square test: $p > 0.05$.

The frequency of the observed genotypes was not different from those expected from the allelic frequencies. The Hardy-Weinberg equilibrium was respected for all markers as shown by chi-square significances.

Figure 8. ***NDUFC2*** **rs641836 polymorphism distribution**

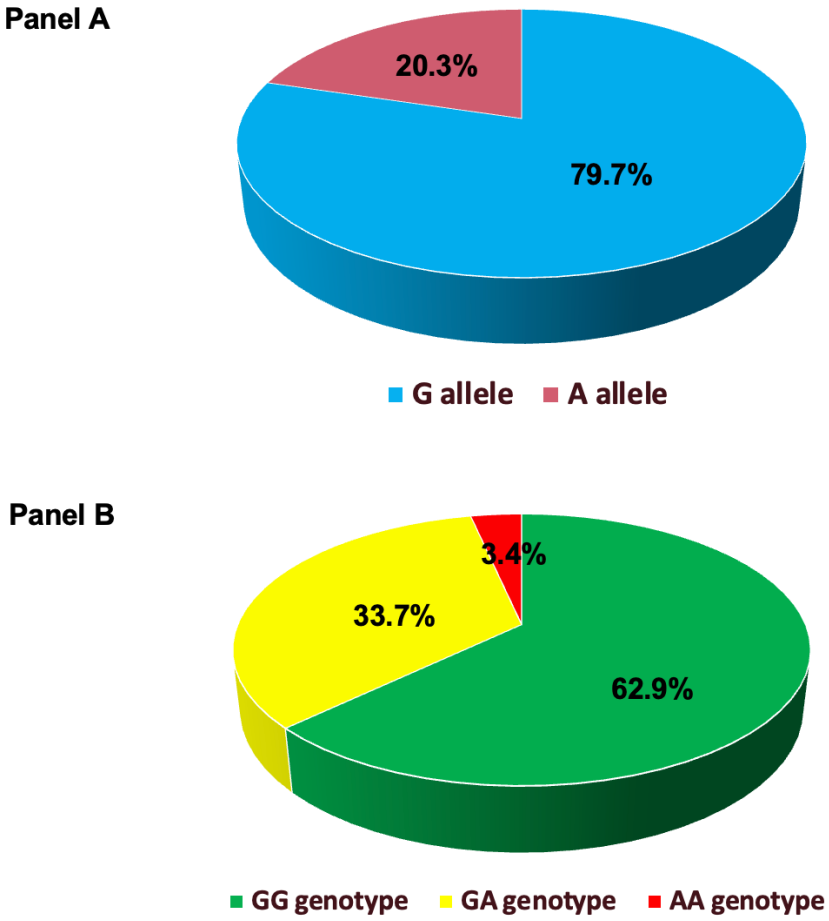

Figure 9. *NDUFC2* rs11237379 polymorphism distribution

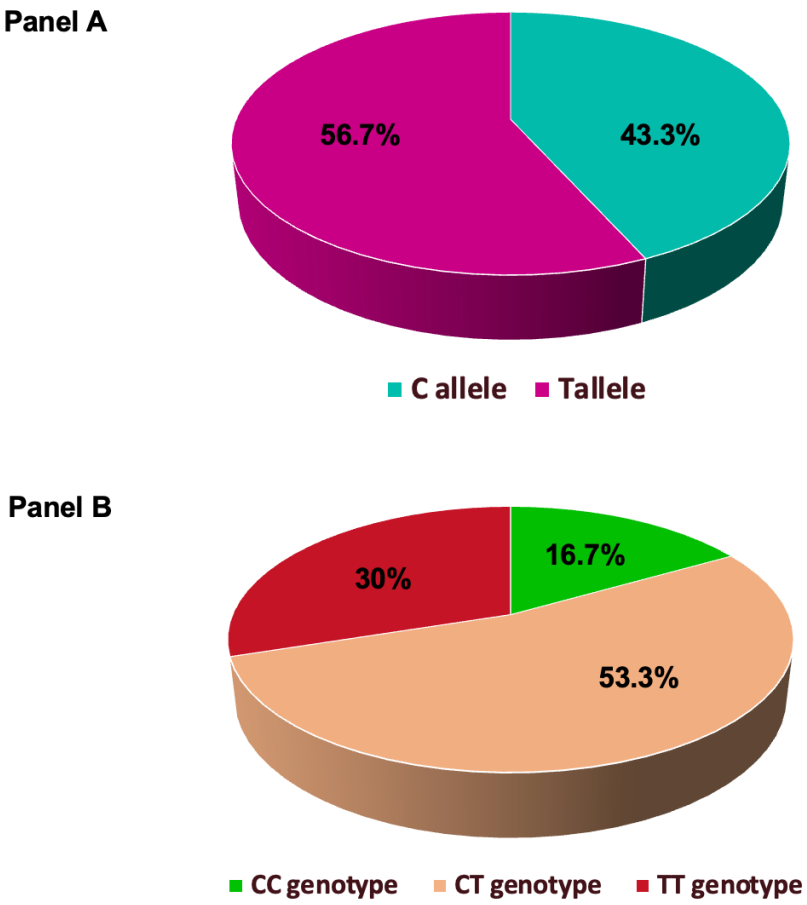

7.a *NDUFC2* rs641836 polymorphism and LVH

Among the whole sample, 146 patients were homozygous for the G allele, 78 patients were heterozygous, and 8 were homozygous for the A allele.

The analysis of possible associations with echocardiographic parameters showed that hypertensive patients who were carriers of the AA genotype had a significantly increase in septal thickness, posterior wall thickness, RWT, LV mass, LV mass/BSA, LV mass/height$^{2.7}$ and LA volume/height^{2} compared to subjects who were carriers of both the AG genotype and GG genotype (Table 3).

To better separate out the genetic effect, a covariate ANOVA was performed for each cardiac variable, considering age, gender, BMI, office BP,

antihypertensive treatment with a combination of 2 or more drugs and the number of BP-lowering agents as covariates. The analysis results were significant for septal thickness, posterior wall thickness, RWT, LV mass, LV mass/BSA and LV mass/height$^{2.7}$ as shown in Table 3 (column titled "Total Model").

Table 3. One-way ANOVA adjusted for the following covariates: age, gender, BMI, BP, combination therapy, number of antihypertensive drugs with the *NDUFC2* rs641836 polymorphism as independent variable

Variables	**GG n=146**	**GA n=78**	**AA n=8**	***NDUFC2* rs641836 p-value; (R^2)**	**Total model p-value; (R^2)**
Septal thickness (mm)	9.8±1.6 %	10.4±1.4 %	12.5±2.0 *#	0.002; (27.3%)	0.006; (17.8%)
LVPW (mm)	9.3±1.4 %#	10.2±1.3 *%	12.2±2.1 *#	0.001; (35.4%)	0.004; (27%)
RWT	0.40±0.06 %	0.42±0.06 %	0.51±0.10 *#	0.001; (18.4%)	0.05; (7.4%)
LV mass (g)	161.7±41.9 %#	186.6±49.4 *%	239.9±67.0 *#	0.001; (39.8%)	0.012; (31.9%)
LV mass/BSA (g/m^2)	87.3±20.1 %#	101.8±24.4 *%	130.1±36.8 *#	0.001; (33.4%)	0.002; (24.6%)

LV mass/$h^{2.7}$ ($g/m^{2.7}$)	37.4±11.6 %	42.4±14.5 %	55.1±10.3 *#	0.006; (24.1%)	0.015; (14.4%)
LA vol/h^2 (ml/m2)	15.1±3.5 %	15.3±2.4 *	24.4±3.6 #	0.022; (11.4%)	0.311; (3.2%)

Legend to Table 3

*<0.05 vs GG; # <0.05 vs GA; %<0.05 vs AA

The column titled *NDUFC2* rs641836 reports the significance (p-value) and amount of variability (R^2) explained by the effect of the Ndufc2 polymorphism independently of all covariates. The column titled Total Model reports the significance (p-value) and amount of variability (R^2) explained by the complete analysis. For abbreviations see Table 1.

Due to the low number of subjects carrying the double mutant allele, individuals carrying the variant allele were joined to confirm the results. Subjects carrying the A mutant allele (n=86) had a significantly increase in septal thickness, posterior wall thickness, RWT, LV mass, LV mass/BSA and LV mass/$height^2$ compared to wild-type homozygotes (Table 4). After the adjustment for the abovementioned covariates the analysis results were significant for posterior wall thickness, LV mass and LV mass/BSA (column titled "Total Model").

Table 4. Echocardiographic variables according to the carrier status of the mutant A allele at *NDUFC2* rs641836.

Variables	GG n=146	GA+AA n=86	*NDUFC2* rs641836 p-value; (R^2)	Total model p-value; (R^2)
Septal thickness (mm)	9.8±1.6	10.6±1.7	0.011; (21.6%)	0.478; (13.9%)
LVPW (mm)	9.3±1.4	10.5±1.5	0.001; (30.4%)	0.013; (23.5%)
RWT	0.40±0.06	0.43±0.06	0.005; (12.1%)	0.287; (3.3%)
LV mass (g)	161.7±41.9	191.2±52.5	0.001; (35.6%)	0.031; (29.2%)
LV mass/BSA (g/m^2)	87.3±20.1	104.3±26.4	0.001; (29.3%)	0.02; (22.2%)
LV mass/$h^{2.7}$ ($g/m^{2.7}$)	37.4±11.6	43.4±14.6	0.01; (16.1%)	0.067; (8%)
LA vol/h^2 (ml/m^2)	15.1±3.5	15.7±3.1	NS	NS

Legend to Table 4.

Each row represents a covaried 1-way analysis of variance of 1 individual cardiac parameter, considered as the dependent variable. The column titled *NDUFC2* rs641836 reports the significance (p-value) and amount of

variability (R^2) explained by the effect of the carrier status of the mutant A allele of Ndufc2 rs641836 independently of all covariates (age, gender, BMI, BP, combination therapy, number of antihypertensive drugs). The column titled Total Model reports the significance (p-value) and amount of variability (R^2) explained by the complete analysis.

7.b *NDUFC2* rs11237379 polymorphism and LVH

Among the whole sample, 39 patients were homozygous for the C allele, 123 patients were heterozygous, and 70 were homozygous for the T allele. The analysis of possible associations with echocardiographic parameters showed that hypertensive patients who were carriers of the TT genotype had a significantly increase in septal thickness, posterior wall thickness, RWT and LV mass/BSA compared to subjects who were carriers of both the CC genotype and CT genotype (Table 5). When a covariate ANOVA was performed, the analysis results were significant for septal and posterior wall thickness, RWT and LV/BSA (column titled "Total Model").

Table 5. One-way ANOVA adjusted for the following covariates: age, gender, BMI, BP, combination therapy, number of antihypertensive drugs with the *NDUFC2* rs11237379 polymorphism as independent variable

Variables	CC N=39	CT N=123	TT N=70	*NDUFC2* rs11237379 p-value; (R^2)	Total model p-value; (R^2)
Septal thickness (mm)	9.7±1.5 %	10.1±1.5	10.8±1.6 *	0.003; (28.8%)	0.027; (20.6%)
LVPW (mm)	9.4±1.4 %	9.6±1.6	10.4±1.7 *	0.004; (29.5%)	0.016; (21.5%)
RWT	0.39±0.05 %	0.41±0.06	0.44±0.07 *	0.01; (25.2%)	0.02; (16.5%)
LV mass (g)	166.4±47.6	168.2±48.8	184.6±46.8	NS	NS
LV mass/BSA (g/m^2)	89.5±24.3 %	89.5±22.1 %	103.0±25.1 *	0.021; (25.5%)	0.04; (16.9%)
LV mass/$h^{2.7}$ ($g/m^{2.7}$)	37.2±12.1	40.9±11.9	43.2±14.5	NS	NS
LA vol/h^2 (ml/m^2)	13.9±1.8	14.9±3.3	16.6±3.9	NS	NS

Legend to Table 5

*<0.05 vs CC; # <0.05 vs CT; %<0.05 vs TT

The column titled Ndufc2 rs11237379 reports the significance (p-value) and amount of variability (R^2) explained by the effect of the *NDUFC*2 polymorphism independently of all covariates. The column titled Total Model reports the significance (p-value) and amount of variability (R^2) explained by the complete analysis. For abbreviations see Table 1.

Subjects carrying both the A allele at *NDUFC2* rs641836 and T allele at *NDUFC2* rs11237379 (n=87) had a significantly increase in septal thickness (p=0.028), posterior wall thickness (p=0.001), RWT (p=0.011), LV mass (p=0.002), LV mass/BSA (p=0.001) and LV mass/height^2 (p=0.0018) compared to those subjects carrying only a mutant allele (n=106) or wild-type (n=39), suggesting an additive role of *NDUFC2* polymorphisms.

8. Discussion

Our data demonstrate the relevance of CI-dependent mitochondrial dysfunction on cardiac hypertrophy development in hypertension and highlight a major role of the SIRT3 pathway as a mechanism mediating the effect of Ndufc2 gene deletion in cardiomyocytes. In this context, NAD+ supplementation, through the correction of the CI deficit, represents an efficacious strategy to counteract cardiac hypertrophy. These findings are consistent with those obtained by previous in vitro mechanistic studies which showed that KO of different CI subunits induced cardiomyocyte hypertrophy, decreased mitochondrial DNA content and MMP, and increased mitochondrial ROS production.

As shown by performing in vitro Ndufc2 silencing in a murine vascular cell line, Ndufc2 is a fundamental component of NADH dehydrogenase to

allow regular CI assembly and activity. Indeed, Ndufc2 deficiency can determine an ultrastructural damage of mitochondria consistent with the functional impairment of CI and with an increased oxidative stress. In fact, its downregulation led to decreased CI integrity and function, decreased mitochondrial membrane potential and ATP production, enhanced ROS accumulation, and inflammation. Consequently, cell viability significantly decreased whereas an increased necrosis was detected (43). Interestingly, the functional significance of Ndufc2 expression was documented by its relationship with an increased stroke susceptibility also in humans (44).

In another study conducted in a model of SHR, the mitochondria of animals with ventricular hypertrophy exhibited impaired enzyme activities of complexes residing on the ETC and decreased protein level of complex subunits, also associated with a dysfunction of the SIRT1/AMPK-PGC-1α axis. A dysregulation in mitochondrial dynamics and mitophagy was also detected. A tendency to fusion rather than fission was observed, resulting in a clustered mitochondrial formation as well as increased average size of mitochondria in the cardiomyocytes (79).

Moreover, in vitro mechanistic studies showed that Ndusf1 KO induced cardiomyocyte hypertrophy, decreased mitochondrial DNA content and increased mitochondrial ROS production, with enhanced expression levels of ANP, BNP, and β-myosin heavy chain. These results were confirmed in Ndusf1-silenced rat cardiomyocytes, supporting the important role of Ndusf1 deletion and, more extensively, of CI dysfunction in the development and progression of cardiac hypertrophy. Further validation by RT-PCR and Western blot showed that the expression levels of Ndusf1 mRNA and protein were downregulated in hypertrophic heart tissue (35).

Another study demonstrated that Ndufs4-null mice had a decrease of about 50% in CI activity within the heart, and developed severe hypertrophic cardiomyopathy as assessed by magnetic resonance imaging (38).

In a model of SHR with LVH mitochondrial protein spots presented significant alterations and the trifunctional enzyme alpha subunit (Hadha) and the CI subunit Ndufa10 were found to have special expression modification patterns (39).

With regard to SIRT3 function, consistently with our findings, previous studies have shown that SIRT3 plays a protective role against mitochondrial damage via regulating the activation of energy metabolism under physiological and pathological conditions. SIRT3 modulates AMPK to protect cardiac function during stress conditions, limiting cellular damage through the modulation of mitochondrial respiration (20,47).

SIRT3 has been previously demonstrated to block cardiac hypertrophy in primary cultures of cardiomyocytes by activating FOXO3a, MnSOD and catalase, thereby decreasing cellular levels of ROS. Reduced ROS levels suppressed Ras activation and downstream signaling through the MAPK/ERK and PI3K/Akt pathways. This resulted in repressed activity of transcription factors, specifically GATA4 and NFAT, and translation factors, specifically eukaryotic initiation factor 4E (elf4E) and P-6SK, which are involved in the development of cardiac hypertrophy (80).

Consistently with previous studies, we found that Ndufc2-silenced cardiomyocytes, compared to not silenced cells, showed a significant degree of hypertrophy by fluorescence microscopy with a significant increase of ANP and β-myosin heavy chain. After the administration of NMN we detected a reduction of cellular volume by fluorescence microscopy and of gene expression level of both hypertrophy markers.

Interestingly, we confirmed the development of cardiac hypertrophy also in Ndufc2-deleted rat neonatal cardiomyocytes and the reduction of cellular area as detected by fluorescence microscopy after NMN supplementation. We found a reduced expression of SIRT3 and of its downstream molecules FOXO3a, MnSOD, phospho-AMPK in Ndufc2-silenced H9c2 cardiomyocytes with a parallel increase of phospho-AKT and of P-6SK. Moreover, SIRT3 level was also reduced in Ndufc2 silenced rat primary cardiomyocytes, thus resulting in cellular hypertrophy as detected by fluorescence microscopy.

With regard to the human study, our results show that *NDUFC*2 polymorphisms, previously demonstrated to produce a significant down-regulation of CI activity (43), are associated with increased cardiac wall thicknesses and LV mass in essential hypertension independently from BP levels as well as from anthropometric and clinical factors. These findings, beside confirming previous experimental evidence, represent the first demonstration in humans of the role played by the CI dysfunction in the process of cardiac remodeling in essential hypertension. Our data provide a good evidence for a biological link underlying the association between *NDUFC*2 polymorphisms and cardiac variables. In fact, we found that the carrier status of the A mutant allele at *NDUFC2* rs641836 and of the TT genotype of *NDUFC2* rs11237379 is associated with an increased risk of LVH. With regard to the biological role of the two *NDUFC*2 markers, previous data showed an association between *NDUFC2* rs11237379 and gene expression (43,44). Therefore, the reduced *NDUFC*2 protein leads to mitochondrial dysfunction, oxidative stress and cardiac hypertrophy. On the other hand, no information is available yet on the

biological role of the *NDUFC2* rs641836. Further studies will be performed to assess it.

Our results provide an excellent translation to humans of experimental findings. They strongly suggest that Ndufc2 deficiency and the consequent CI dependent mitochondrial dysfunction play an important contributory role for LVH development in hypertensive patients. Additional studies are certainly required to reinforce the current findings and their potential great relevance for prevention and treatment of hypertensive cardiac damage.

9. References

1) Nakamura M, Sadoshima J. Mechanisms of physiological and pathological cardiac hypertrophy. Nat Rev Cardiol. 2018 Jul;15(7):387-407
2) Lorell BH, Carabello BA. Left ventricular hypertrophy: pathogenesis, detection, and prognosis. Circulation. 2000 Jul 25;102(4):470-9
3) Frohlich E, Gonzales A, Diez J. Hypertensive left ventricular hypertrophy risk: beyond adaptive cardiomyocytic hypertrophy. J Hypertens 2011; 29: 17 -- 26.
4) Shimizu I, Minamino T. Physiological and pathological cardiac hypertrophy. J Mol Cell Cardiol. 2016 Aug;97:245-62
5) Samak M, Fatullayev J, Sabashnikov A, Zeriouh M, Schmack B, Farag M, Popov AF, Dohmen PM, Choi YH, Wahlers T, Weymann A. Cardiac Hypertrophy: An Introduction to Molecular and Cellular Basis. Med Sci Monit Basic Res. 2016 Jul 23;22:75-9
6) Kehat I, Molkentin JD. Molecular pathways underlying cardiac remodeling during pathophysiological stimulation. Circulation 2010; 122: 2727 -- 2735.

7) Lips DJ, deWindt LJ, van Kraaij DJW, et al. Molecular determinants of myocardial hypertrophy and failure: alternative pathways for beneficial and maladaptive hypertrophy. Eur Heart J 2003;24:883–96.
8) Swynghedauw B. Molecular mechanisms of myocardial remodeling. Physiol Rev. 1999;79:216 –261.
9) Lam CSP, Voors AA, de Boer RA, Solomon SD, van Veldhuisen DJ. Heart failure with preserved ejection fraction: from mechanisms to therapies. Eur Heart J. 2018 Aug 7;39(30):2780-2792
10) Imamura T, McDermott PJ, Kent RL, et al. Acute changes in myosin heavy chain synthesis rate in pressure versus volume overload. Circ Res. 1994;75:418–425
11) Oldfield CJ, Duhamel TA, Dhalla NS. Mechanisms for the transition from physiological to pathological cardiac hypertrophy. Can J Physiol Pharmacol. 2020 Feb;98(2):74-84
12) Chung CS, Granzier HL. Contribution of titin and extracellular matrix to passive pressure and measurement of sarcomere length in the mouse left ventricle. J Mol Cell Cardiol 2011;50:731–739.
13) LeWinter MM. Myocardial stiffness in patients with heart failure and a preserved ejection fraction: contributions of collagen and titin. Circulation 2015; 131:1247–1259.
14) Kuppuswamy D, Kerr C, Narishige T, Kasi VS, Menick DR, Cooper G 4th. Association of tyrosine-phosphorylated c-Src with the cytoskeleton of hypertrophying myocardium. J Biol Chem. 1997 Feb 14;272(7):4500-8
15) Terracio L, Rubin K, Gullberg D, Balog E, Carver W, Jyring R, Borg TK. Expression of collagen binding integrins during cardiac development and hypertrophy. Circ Res. 1991 Mar;68(3):734-44

16) Sadoshima JI, Izumo S. Molecular characterization of angiotensin II-induced hypertrophy of cardiac myocytes and hyperplasia of cardiac fibroblasts. Circ Res. 1993;73:413– 423

17) Singh MV, Cicha MZ, Nunez S, Meyerholz DK, Chapleau MW, Abboud FM. Angiotensin II-induced hypertension and cardiac hypertrophy are differentially mediated by TLR3- and TLR4-dependent pathways. Am J Physiol Heart Circ Physiol. 2019 May 1;316(5):H1027-H1038

18) Harada K, Komuro I, Shiojima I, et al. Pressure overload induces cardiac hypertrophy in angiotensin II type 1A receptor knockout mice. Circulation. 1998;97:1952–1959.

19) Molkentin JD, Lu JR, Antos CL, Markham B, Richardson J, Robbins J, Grant SR, Olson EN. A calcineurin-dependent transcriptional pathway for cardiac hypertrophy. Cell. 1998 Apr 17;93(2):215-28

20) Zhang W, Kowal RC, Rusnak F, Sikkink RA, Olson EN, Victor RG. Failure of calcineurin inhibitors to prevent pressure-overload left ventricular hypertrophy in rats. Circ Res. 1999 Apr 2;84(6):722-8

21) Homcy CJ. Signaling hypertrophy: how many switches, how many wires? Circulation. 1998;97:1890 –1892

22) Creemers EE, Pinto YM. Molecular mechanisms that control interstitial fibrosis in the pressure-overloaded heart. Cardiovasc Res 2011;89:265–272.

23) Leask A. Getting to the heart of the matter: new insights into cardiac fibrosis. Circ Res 2015;116:1269–1276.

24) Schlaich MP, Kaye DM, Lambert E, Sommerville M, Socratous F, Esler MD. Relation between cardiac sympathetic activity and

hypertensive left ventricular hypertrophy. Circulation. 2003 Aug 5;108(5):560-5

25) Kuwahara F, Kai H, Tokuda K, Takeya M, Takeshita A, Egashira K, Imaizumi T. Hypertensive myocardial fibrosis and diastolic dysfunction. Hypertension 2004; 43:739–745.

26) van Heerebeek L, Franssen CP, Hamdani N, Verheugt FW, Somsen GA, Paulus WJ. Molecular and cellular basis for diastolic dysfunction. Curr Heart Fail Rep 2012;9:293–302.

27) Rosca MG, Tandler B, Hoppel CL. Mitochondria in cardiac hypertrophy and heart failure. J Mol Cell Cardiol. 2013 Feb;55:31-41

28) Karamanlidis G, Lee CF, Garcia-Menendez L, Kolwicz SC, Suthammarak W, Gong G, Sedensky MM, Morgan PG, Wang W, Tian R, Kolwicz SC, Jr, Suthammarak W, Gong G, Sedensky MM, Morgan PG, Wang W, Tian R. Mitochondrial complex i deficiency increases protein acetylation and accelerates heart failure. Cell Metab. 2013;18:239–250.

29) Osterholt M, Nguyen TD, Schwarzer M, Doenst T. Alterations in mitochondrial function in cardiac hypertrophy and heart failure. Heart Fail Rev 2013;18:645–56.

30) Rubattu S, Stanzione R, Volpe M. Mitochondrial Dysfunction Contributes to Hypertensive Target Organ Damage: Lessons from an Animal Model of Human Disease. Oxid Med Cell Longev. 2016;2016:1067801.

31) Peoples JN, Saraf A, Ghazal N, Pham TT, Kwong JQ. Mitochondrial dysfunction and oxidative stress in heart disease. Exp Mol Med. 2019 Dec 19;51(12):1-13

32) Wirth C, Brandt U, Hunte C, Zickermann V. Structure and function of mitochondrial complex I. Biochim Biophys Acta. 2016 Jul;1857(7):902-14.

33) Takimoto E, Kass DA. Role of oxidative stress in cardiac hypertrophy and remodeling. Hypertension. 2007 Feb;49(2):241-8

34) Ni Y, Hagras MA, Konstantopoulou V, Mayr JA, Stuchebrukhov AA, Meierhofer D. Mutations in NDUFS1 Cause Metabolic Reprogramming and Disruption of the Electron Transfer. Cells. 2019 Sep 25;8(10):1149

35) Zou R, Tao J, Qiu J, Shi W, Zou M, Chen W, Li W, Zhou N, Wang S, Ma L, Chen X. Ndufs1 Deficiency Aggravates the Mitochondrial Membrane Potential Dysfunction in Pressure Overload-Induced Myocardial Hypertrophy. Oxid Med Cell Longev. 2021 Mar 3;2021:5545261

36) Schwartz F, Duka A, Duka I, Cui J, Gavras H. Novel targets of ANG II regulation in mouse heart identified by serial analysis of gene expression. Am J Physiol Heart Circ Physiol. 2004 Nov;287(5):H1957-66

37) Qi Y, Wang X, Rose KL, MacDonald WH, Zhang B, Schey KL, Luther JM. Activation of the Endogenous Renin-Angiotensin-Aldosterone System or Aldosterone Administration Increases Urinary Exosomal Sodium Channel Excretion. J Am Soc Nephrol. 2016 Feb;27(2):646-56

38) Chouchani ET, Methner C, Buonincontri G, Hu CH, Logan A, Sawiak SJ, Murphy MP, Krieg T. Complex I deficiency due to selective loss of Ndufs4 in the mouse heart results in severe hypertrophic cardiomyopathy. PLoS One. 2014 Apr 4;9(4):e94157

39) Meng C, Jin X, Xia L, Shen SM, Wang XL, Cai J, Chen GQ, Wang LS, Fang NY. Alterations of mitochondrial enzymes contribute to cardiac hypertrophy before hypertension development in spontaneously hypertensive rats. J Proteome Res. 2009 May;8(5):2463-75

40) Lehman JJ, Kelly DP. Transcriptional activation of energy metabolic switches in the developing and hypertrophied heart. Clin Exp Pharmacol Physiol. 2002 Apr;29(4):339-45

41) Huss JM, Kelly DP. Mitochondrial energy metabolism in heart failure: a question of balance. J Clin Invest. 2005 Mar;115(3):547-55.

42) Gershoni M, Levin L, Ovadia O, Toiw Y, Shani N, Dadon S, Barzilai N, Bergman A, Atzmon G, Wainstein J, Tsur A, Nijtmans L, Glaser B, Mishmar D. Disrupting mitochondrial-nuclear coevolution affects OXPHOS complex I integrity and impacts human health. Genome Biol Evol. 2014 Sep 22;6(10):2665-80

43) Raffa S, Scrofani C, Valente S, Micaloni A, Forte M, Bianchi F, Coluccia R, Geurts AM, Sciarretta S, Volpe M, Torrisi MR, Rubattu S. In vitro characterization of mitochondrial function and structure in rat and human cells with a deficiency of the NADH: ubiquinone oxidoreductase Ndufc2 subunit. Hum Mol Genet. 2017 Dec 1;26(23):4541-4555

44) Rubattu S, Di Castro S, Schulz H, Geurts AM, Cotugno M, Bianchi F, Maatz H, Hummel O, Falak S, Stanzione R, Marchitti S, Scarpino S, Giusti B, Kura A, Gensini GF, Peyvandi F, Mannucci PM, Rasura M, Sciarretta S, Dwinell MR, Hubner N, Volpe M. Ndufc2 Gene Inhibition Is Associated With Mitochondrial Dysfunction and Increased Stroke Susceptibility in an Animal Model of Complex Human Disease. J Am Heart Assoc. 2016 Feb 17;5(2):e002701.

45) Haigis MC, Sinclair DA. Mammalian sirtuins: biological insights and disease relevance. Annu Rev Pathol. 2010;5:253–295.

46) Imai S ichiro, Guarente L. NAD+ and sirtuins in aging and disease. Trends Cell Biol. 2014;24:464–471.

47) Kane AE, Sinclair DA. Sirtuins and NAD+ in the Development and Treatment of Metabolic and Cardiovascular Diseases. Circ Res. 2018 Sep 14;123(7):868-885.

48) Vaziri H, Dessain S, Ng Eaton E, Imai S, Frye R, Pandita T, Guarente L, Weinberg R. SIRT1 functions as an NAD-dependent p53 deacetylase. Cell. 2001;107:149–159

49) Planavila A, Iglesias R, Giralt M, Villarroya F. Sirt1 acts in association with PPARα to protect the heart from hypertrophy, metabolic dysregulation, and inflammation. Cardiovasc Res 2011;90:276–84.

50) Chang HC, Guarente L. SIRT1 and other sirtuins in metabolism. Trends Endocrinol Metab. 2014;25:138–145.

51) Rodgers JT, Lerin C, Haas W, Gygi SP, Spiegelman BM, Puigserver P. Nutrient control of glucose homeostasis through a complex of PGC-1a and SIRT1. Nature. 2005;434:113–118.

52) Cantó C, Gerhart-Hines Z, Feige JN, Lagouge M, Noriega L, Milne JC, Elliott PJ, Puigserver P, Auwerx J. AMPK regulates energy expenditure by modulating NAD + metabolism and SIRT1 activity. Nature. 2009;458:1056–1060

53) Huh JE, Shin JH, Jang ES, Park SJ, Park DR, Ko R, Seo DH, Kim HS, Lee SH, Choi Y, Kim HS, Lee SY. Sirtuin 3 (SIRT3) maintains bone homeostasis by regulating AMPK-PGC-1β axis in mice. Sci Rep. 2016 Mar 1;6:22511

54) Parodi-Rullán RM, Chapa-Dubocq X, Rullán PJ, Jang S, Javadov S. High Sensitivity of SIRT3 Deficient Hearts to Ischemia-Reperfusion Is Associated with Mitochondrial Abnormalities. Front Pharmacol. 2017 May 16;8:275

55) Samant SA, Zhang HJ, Hong Z, Pillai VB, Sundaresan NR, Wolfgeher D, Archer SL, Chan DC, Gupta MP. SIRT3 deacetylates and activates OPA1 to regulate mitochondrial dynamics during stress. Mol Cell Biol. 2014 Mar;34(5):807-19

56) Sun W, Liu C, Chen Q, Liu N, Yan Y, Liu B. SIRT3: A New Regulator of Cardiovascular Diseases. Oxid Med Cell Longev. 2018 Feb 13;2018:7293861.

57) Tseng AH, Shieh SS, Wang DL. SIRT3 deacetylates FOXO3 to protect mitochondria against oxidative damage. Free Radic Biol Med. 2013 Oct;63:222-34

58) Zhao W, Zhang L, Chen R, Lu H, Sui M, Zhu Y, Zeng L. SIRT3 Protects Against Acute Kidney Injury via AMPK/mTOR-Regulated Autophagy. Front Physiol. 2018 Nov 14;9:1526

59) Hirschey MD, Shimazu T, Goetzman E, Jing E, Lombard DB, Grueter C a, Harris C, Biddinger S, Ilkayeva OR, Stevens RD, Li Y, Saha AK, Ruderman NB, James R, Newgard CB, RVF Jr, Alt FW, Kahn CR, Verdin E. SIRT3 regulates fatty acid oxidation via reversible enzyme deacetylation. Nature. 2010;464:121–125.

60) Sundaresan N, Bindu S, Pillai V, Saman S, Pan Y, Huang J, Gupta M, Nagalingam R, Wolfgether D, Verdin E, Cgupta M. SIRT3 blocks aging-associated tissue fibrosis in mice by deacetylating and activating glycogen synthase kinase 3 β. Mol Cell Biol. 2016;36:678–692.

61) 148. Sundaresan NR, Gupta M, Kim G, Rajamohan SB, Isbatan A, Gupta MP. Sirt3 blocks the cardiac hypertrophic response by augmenting Foxo3a-dependent antioxidant defense mechanisms in mice. J Clin Invest. 2009;119:2758–2771. [PubMed: 19652361]

62) 149. Samant SA, Zhang HJ, Hong Z, Pillai VB, Sundaresan NR, Wolfgeher D, Archer SL, Chan DC, Gupta MP. SIRT3 Deacetylates and Activates OPA1 To Regulate Mitochondrial Dynamics during Stress. Mol Cell Biol. 2014;34:807–819. [PubMed: 24344202]

63) Pillai VB, Sundaresan NR, Kim G, Gupta M, Rajamohan SB, Pillai JB, Samant S, Ravindra P V., Isbatan A, Gupta MP. Exogenous NAD blocks cardiac hypertrophic response via activation of the SIRT3-LKB1-AMP-activated kinase pathway. J Biol Chem. 2010;285:3133–3144.

64) Chen T, Li J, Liu J, Li N, Wang S, Liu H, Zeng M, Zhang Y, Bu P. Activation of SIRT3 by resveratrol ameliorates cardiac fibrosis and improves cardiac function via the TGF-β/Smad3 pathway. Am J Physiol - Hear Circ Physiol. 2015;308:H424–H434.

65) Zhang J, He Z, Fedorova J, Logan C, Bates L, Davitt K, Le V, Murphy J, Li M, Wang M, Lakatta EG, Ren D, Li J. Alterations in mitochondrial dynamics with age-related Sirtuin1/Sirtuin3 deficiency impair cardiomyocyte contractility. Aging Cell. 2021 Jul;20(7):e13419

66) Papanicolaou KN, Ngoh GA, Dabkowski ER, O'Connell KA, Ribeiro RF Jr, Stanley WC, Walsh K. Cardiomyocyte deletion of mitofusin-1 leads to mitochondrial fragmentation and improves tolerance to ROS-induced mitochondrial dysfunction and cell death. Am J Physiol Heart Circ Physiol. 2012 Jan 1;302(1):H167-79.

67) Chen Y, Csordás G, Jowdy C, Schneider TG, Csordás N, Wang W, Liu Y, Kohlhaas M, Meiser M, Bergem S, Nerbonne JM, Dorn GW 2nd, Maack C. Mitofusin 2-containing mitochondrial-reticular microdomains direct rapid cardiomyocyte bioenergetic responses via interorganelle Ca(2+) crosstalk. Circ Res. 2012 Sep 14;111(7):863-75

68) Lombard DB, Alt FW, Cheng HL, Bunkenborg J, Streeper RS, Mostoslavsky R, Kim J, Yancopoulos G, Valenzuela D, Murphy A, Yang Y, Chen Y, Hirschey MD, Bronson RT, Haigis M, Guarente LP, Farese RV Jr, Weissman S, Verdin E, Schwer B. Mammalian Sir2 homolog SIRT3 regulates global mitochondrial lysine acetylation. Mol Cell Biol. 2007 Dec;27(24):8807-14

69) Yu W, Gao B, Li N, Wang J, Qiu C, Zhang G, Liu M, Zhang R, Li C, Ji G, Zhang Y. Sirt3 deficiency exacerbates diabetic cardiac dysfunction: Role of Foxo3A-Parkin-mediated mitophagy. Biochim Biophys Acta - Mol Basis Dis. 2017;1863:1973–1983.

70) Pillai VB, Samant S, Sundaresan NR, Raghuraman H, Kim G, Bonner MY, Arbiser JL, Walker DI, Jones DP, Gius D, Gupta MP. Honokiol blocks and reverses cardiac hypertrophy in mice by activating mitochondrial SIRT3. Nat Commun. 2015;6:6656.

71) Porter GA, Urciuoli WR, Brookes PS, Nadtochiy SM. SIRT3 deficiency exacerbates ischemia-reperfusion injury: implication for aged hearts. AJP Hear Circ Physiol. 2014;306:H1602–H1609.

72) Hsu C-P, Zhai P, Yamamoto T, Maejima Y, Matsushima S, Hariharan N, Shao D, Takagi H, Oka S, Sadoshima J. Sirt1 Protects the Heart from Ischemia Reperfusion. Circulation. 2010;122:2170–2182.

73) Pillai VB, Sundaresan NR, Gupta MP. Regulation of Akt signaling by sirtuins: its implication in cardiac hypertrophy and aging. Circ Res. 2014 Jan 17;114(2):368-78.

74) Sundaresan NR, Gupta M, Kim G, Rajamohan SB, Isbatan A, Gupta MP. Sirt3 blocks the cardiac hypertrophic response by augmenting Foxo3a-dependent antioxidant defense mechanisms in mice. J Clin Invest. 2009 Sep;119(9):2758-71.

75) Kar D, Bandyopadhyay A. Targeting Peroxisome Proliferator Activated Receptor α (PPAR α) for the Prevention of Mitochondrial Impairment and Hypertrophy in Cardiomyocytes. Cell Physiol Biochem. 2018;49(1):245-259

76) Sciarretta S, Yee D, Nagarajan N, Bianchi F, Saito T, Valenti V, Tong M, Del Re DP, Vecchione C, Schirone L, Forte M, Rubattu S, Shirakabe A, Boppana VS, Volpe M, Frati G, Zhai P, Sadoshima J. Trehalose-Induced Activation of Autophagy Improves Cardiac Remodeling After Myocardial Infarction. J Am Coll Cardiol. 2018 May 8;71(18):1999-2010

77) Lang RM, Badano LP, Mor-Avi V, Afilalo J, Armstrong A, Ernande L, Flachskampf FA, Foster E, Goldstein SA, Kuznetsova T, Lancellotti P, Muraru D, Picard MH, Rietzschel ER, Rudski L, Spencer KT, Tsang W, Voigt JU. Recommendations for cardiac chamber quantification by echocardiography in adults: an update from the American Society of Echocardiography and the European Association of Cardiovascular Imaging. J Am Soc Echocardiogr. 2015 Jan;28(1):1-39.e14

78) Williams B, Mancia G, Spiering W, Agabiti Rosei E, Azizi M, Burnier M, Clement DL, Coca A, de Simone G, Dominiczak A, Kahan T,

Mahfoud F, Redon J, Ruilope L, Zanchetti A, Kerins M, Kjeldsen SE, Kreutz R, Laurent S, Lip GYH, McManus R, Narkiewicz K, Ruschitzka F, Schmieder RE, Shlyakhto E, Tsioufis C, Aboyans V, Desormais I; ESC Scientific Document Group. 2018 ESC/ESH Guidelines for the management of arterial hypertension. Eur Heart J 2018;39:3021-3104.

79) Tang Y, Mi C, Liu J, Gao F, Long J. Compromised mitochondrial remodeling in compensatory hypertrophied myocardium of spontaneously hypertensive rat. Cardiovasc Pathol. 2014 Mar-Apr;23(2):101-6

80) Sundaresan NR, Gupta M, Kim G, Rajamohan SB, Isbatan A, Gupta MP. Sirt3 blocks the cardiac hypertrophic response by augmenting Foxo3a-dependent antioxidant defense mechanisms in mice. J Clin Invest. 2009 Sep;119(9):2758-71